ECS Transactions, 45 (1) 405-412 (2012)
10.1149/1.3701331 ©The Electrochemical Society

Role of Chemical Heterogeneities on Oxygen Reduction Kinetics on the Surface of Thin Film Cathodes

Wonyoung Lee, Zhuhua Cai, and Bilge Yildiz

Laboratory of Electrochemical Interfaces
Department of Nuclear Science and Engineering, Massachusetts Institute of Technology, Cambridge, MA 02139, USA

We investigated the effects of annealing and A-site stoichiometry on the surface heterostructures at $(La_{0.8}Sr_{0.2})_yMnO_3$ (LSM, $y \leq 1$) dense thin films. While annealing at the high temperature induces cation segregation on LSM, A-site deficiency is hypothesized to reduce the level of Sr enrichment on the surface upon annealing by providing more space in the bulk of LSM for this relatively large cation. Localized chemical analysis by nano-probe Auger electron spectroscopy revealed the strong enrichment of Sr and Zr in particles that form on the surface of LSM films upon annealing. By systematically varying y from 1.0 to 0.95, A-site deficiency in LSM films was shown to suppress the Sr segregation on the surface and to decrease the particle density of these secondary phases on the surface of the annealed LSM films, suggesting a higher chemical stability of LSM surface with A-site deficiency. Our results contribute to understanding the elastic energy contributions to cation segregation on the surface of perovskite cathodes, and to elucidating the role of surface chemical heterogeneities to the ORR kinetics.

Introduction

The slow rate of oxygen reduction reaction (ORR) at the cathode is one of the main barriers for implementation of high-performance solid oxide fuel cells (SOFCs) at intermediate temperatures (500-700 °C) (1). It is generally agreed that the ORR kinetics is limited by the surface exchange reactions on the surface of mixed ionic electronic oxide cathodes. The structural, chemical and electrochemical properties of the cathode surface are of importance to improve the ORR reactivity. However, the dynamic nature of surface structure and chemistry, driven by the harsh conditions of high temperatures and oxygen partial pressure in SOFCs, has resulted in difficulties to probe and fundamentally understand the origin of the activation and deactivation of ORR kinetics on the surfaces (2). Although cation segregation and phase separation on the surface of perovskite oxides has been commonly observed (3,4) the driving forces to cation segregation and its impact on the surface electrochemical activity remains yet controversial. In this work, we show the effect of annealing on the structure and cation chemistry at the $(La_{0.8}Sr_{0.2})_yMnO_3$ (LSM) surface as a model cathode system. The A-site stoichiometry was varied systematically to assess how the surface segregation of Sr and the consequent formation of secondary phases on the surface are influenced by the

chemical composition of LSM thin films. Here the hypothesis is that the excess available cation sub-lattice space in the bulk of an A-site deficient LSM structure can accommodate the relatively large Sr cation more easily in the bulk, by considerations of elastic energy minimization, and reduce the Sr segregation and phase separation on the surface. While the elastic energy term is expected to act along with electrostatic and cohesive energy terms on the cation segregation thermodynamics, here we isolate only the elastic energy contribution by varying the A-site deficiency and assume a uniform distribution of A-site cation vacancies in the films. High resolution characterization of surface structure and localized chemical composition was performed to identify cation chemistry, bonding states, and structure of the annealing-induced particles. On the basis of our experimental results, we discuss the possible mechanisms for segregation and secondary phase formation at the LSM film surfaces. These results contribute to understanding the role of elastic energy contributions to cation segregation on the surface of perovskite cathodes, and to elucidating the role of surface chemical heterogeneities to the ORR kinetics.

Experimental Methods

Three sets of LSM thin films were fabricated with the same structure but different A-site content, $(La_{0.8}Sr_{0.2})_yMnO_3$ with y = 1.0 (LSM100), 0.98 (LSM98) and 0.95 (LSM95). LSM thin films with a thickness of about 20 nm were deposited on single-crystal yttria-stabilized zirconia (YSZ) (100) substrates using pulsed laser deposition with a KrF excimer laser at a wavelength of 248 nm and laser beam energy of 550 mJ/pulse at 10 Hz. The deposition was performed at 815 ºC with oxygen pressure of 20 mTorr and with the target-to-substrate distance of 6 cm. After deposition, the sample was cooled at 10 °C/min to room temperature in an oxygen pressure of 10 Torr.

A Veeco/Digital Instrument Nanoscope IV was used to perform tapping mode atomic force microscopy (AFM) for characterizing the surface morphology. X-ray photoelectron spectroscopy (XPS) was used to probe the surface cation chemistry and bonding states. The Omicron EA 125 hemispherical analyzer and Omicron DAR 400 Mg/Al dual anode nonmonochromated X-ray source were used for measurements, and CasaXPS 2.3.15 software was used for peak analysis and quantification. Spectra were acquired with emission angles from 0 ° to 80 ° as defined relative to the surface normal. The Sr 3d, La 3d and Mn 2p core emissions were measured with two emission angles of θ = 0 ° and 80 °. For the excitation energy of 1253.6 eV, the sampling depths of these photoelectrons at 0 ° emission angle are ~6 nm for Sr 3d, La 4d, and Zr 3d, ~3 nm for La 3d, ~4 nm for Mn 2p (5). At the emission angle of 80 °, the measurements are more surface sensitive because the sampling depths of each element are about 20% of those at the emission angle of 0 °. As-deposited samples were measured after cleaning at 500-550 ºC for 1 hr in $\sim 5\times10^{-5}$ mbar of oxygen in the UHV chamber. After annealing at 750 ºC for 4 hrs in air, samples were quenched to preserve the surface state at elevated temperature. A Physical

Electronics Model 700 Scanning nano-probe Auger electron spectroscopy (NAES) was used to identify the surface cation content with the ability to detect lateral heterogeneities in cation compositions with high spatial resolution. Incident electron beam of 20 keV and 10 nA were used for both secondary electron microscopy (SEM) imaging and the Auger electron excitation. The La MNN, Sr LMM, Mn LMM, and Zr MNN Auger emissions were measured for quantifying the surface cation composition of the LSM films. The sampling depths of these AES electrons are ~8 nm for Sr LMM, ~4 nm for La MNN and Mn LMM, and ~2 nm for Zr MNN (5).

Results and Discussion

Surface structure of LSM thin films

Figure 1 shows the phase images of the LSM100 surface using tapping mode AFM. As-deposited surface showed very uniform and smooth topography with an RMS roughness of less than 1 nm. After annealing at 750 ºC for 4 hr in air, particles with a height of 5-50 nm and a width of 50-200 nm appeared on the surface, consistently with previous reports (6,7). LSM surface grains became greater in size, resulting in the increase of an RMS roughness to 15-20 nm. Figure 2 shows the surface morphology (SEM imaging) of annealed LSM samples with varying A-site stoichiometry. The particle density showed a clear trend; the LSM sample surface with higher A-site deficiency had a lower particle density. Formation of fewer particles may indicate the improved chemical stability of the LSM films with higher A-site deficiency. Accordingly, we conclude that 1) annealing induced structural changes, particle formation, on the surface, and 2) A-site stoichiometry affected the particle density, but not the dimension or shape of the particles.

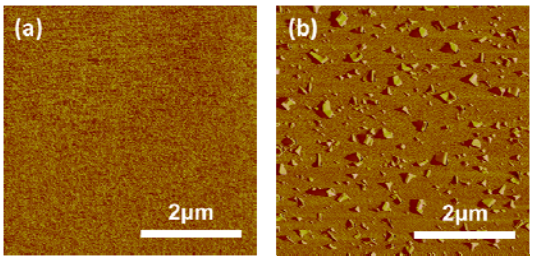

Figure 1. The phase images of (a) as-deposited and (b) annealed LSM100 surfaces.

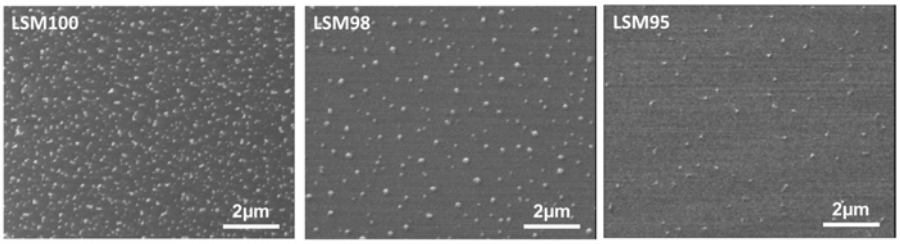

Figure 2. SEM images of annealed LSM sample surfaces. (a) LSM100, (b) LSM98, and (c) LSM95.

Surface cation chemistry with angle-resolved XPS

XPS spectra of Sr 3d core level emissions contain two components, arising from the lattice ($Sr_{lattice}$) and from the surface ($Sr_{surface}$) (8,9). For the as-deposited samples, the ratio, $Sr_{surface}/Sr_{lattice}$, increased at larger emission angles, as summarized in Table 1. The increase of $Sr_{surface}/Sr_{lattice}$ with the emission angle indicates the higher concentration of Sr on the surface. Sr segregation on the surface was supported by the increase of cation intensity ratio, Sr/Mn, with the increase of the emission angle from 0 ° to 80 °. Sr segregation was observed on all of the as-deposited LSM samples in this work. However, the $Sr_{surface}/Sr_{lattice}$ ratio decreased with A-site deficiency at both emission angles, indicating less Sr segregation with the higher A-site deficiency in LSM films.

Table 1. Relative chemical content on the surface of LSM films from XPS analysis.

Atomic ratio	Sample	As-deposited		Annealed	
		θ = 0°	θ = 80°	θ = 0°	θ = 80°
$Sr_{surface}$ / $Sr_{lattice}$	LSM100	0.30	0.40	1.29	6.81
	LSM98	0.27	0.37	1.82	5.68
	LSM95	0.11	0.22	0.59	1.97
Sr / Mn	LSM100	0.70	1.58	0.66	2.46
	LSM98	0.73	1.46	0.79	2.37
	LSM95	0.68	1.49	0.56	1.07

$Sr_{surface}/Sr_{lattice}$ and Sr/Mn ratios significantly increased upon annealing. The increase was more pronouncedly detected with the emission angle of 80 °, indicating that significant Sr segregation occurred on the surface. Another substantial change upon annealing was Zr interdiffusion from the YSZ substrates (10) into/onto the LSM films with an atomic concentration of Zr 30 % on LSM100 and 20% on LSM98, measured at 80 °. Higher concentration of Sr and Zr after annealing was concurrent with the appearance of particles on the surfaces as shown in Figure 1 and Figure 2. Concomitant chemical changes with the appearance of new surface structures suggest that these particles are mainly composed of Sr and Zr.

Localized surface cation chemistry with AES

In order to determine the structure and chemistry of such heterogeneities on the surface, localized chemical information is required. Figure 3 shows the elemental maps of annealed LSM sample surfaces measured by nano-probe AES. Brighter color represents higher intensity of each element. Higher intensities of Sr and Zr (and lower intensities of La and Mn) on particles compared to the particle-free regions of the surface on the LSM films reveal that these secondary phase particles have a higher concentration of Sr and Zr.

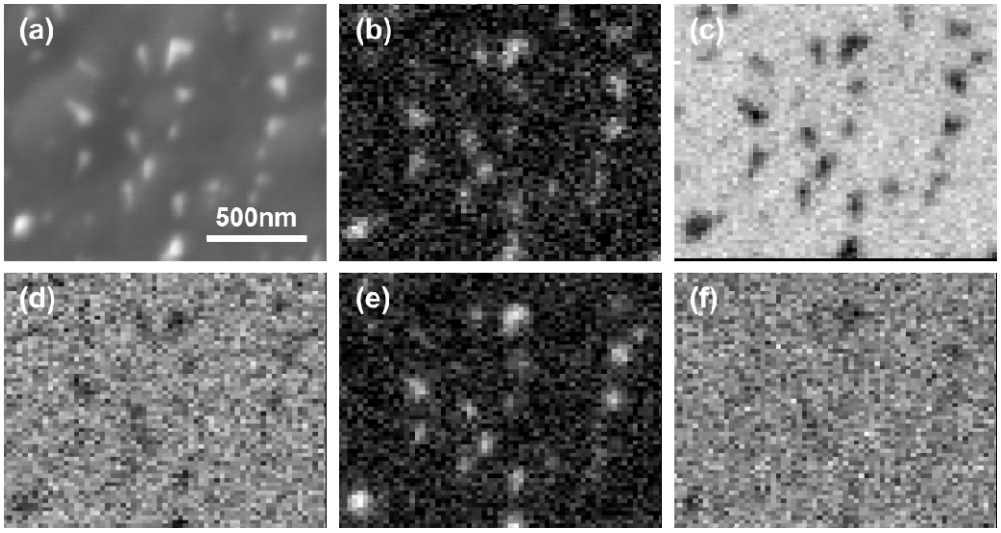

Figure 3. (a) SEM image, and the AES elemental maps deduced from the (b) Sr LMM, (c) La MNN, (d) Mn LMM, (e) Zr MNN, and (f) O KLL peaks on the annealed LSM100 films.

Figure 4 shows the cation intensity ratios normalized by Mn peaks from the high resolution Auger electron spectra on each of LSM100, LSM98, and LSM95. As-deposited LSM samples have similar Sr/Mn and La/Mn ratios. On the annealed samples, AES spectra were acquired from two locations; on top of particles (ON-particle), and away from particles (OFF-particle). The most significant change is the increase of Sr/Mn ON-particle, while a small decrease of Sr/Mn is found OFF-particle. The increase of Zr/Mn is more pronounced ON-particle compared to OFF-particle. La/Mn increases after annealing with the similar values for ON- and OFF-particle. This can be explained by observation from Figure 3 that Mn intensity decreased for both ON- and OFF-particle, whereas La intensity increased OFF-particle but decreased ON-particle. Combination of the absolute elemental intensity and concentration ratios reveals the localized chemical heterogeneities on the annealed LSM thin films; 1) annealing-induced particles (ON-particle) have more Sr and Zr, but less Mn and La, and 2) LSM surfaces away from the particles (OFF-particle) have more Zr and La, but less Sr and Mn, as compared to the as-deposited LSM surfaces. It should be noted that the difference between ON- and OFF-particle regions in Sr/Mn and Zr/Mn reduced noticeably in LSM95 samples. This indicates that the LSM95 is more stable against Sr-enrichment on the surface and formation of such Sr- and Zr-rich particles upon annealing than the LSM100 and LSM98.

These localized chemical compositions from AES, the particle densities from SEM, and the particle geometries from AFM allow more interpretation of the XPS results in Table 1. With the higher A-site deficiency in LSM films (in particular the LSM95), the $Sr_{surface}/Sr_{lattice}$ and Sr/Mn ratio decreased on the surface (at 80 °). The decrease of $Sr_{surface}/Sr_{lattice}$ can be attributed to the decrease of the particle density on the surface. Because particles have similar geometry and significant Sr-enrichment, the lower particle density on LSM98 and LSM95 results in the decrease of $Sr_{surface}/Sr_{lattice}$. The decrease of

Sr/Mn from XPS can be also explained by the same reason, lower particle density. Interestingly, the subtle change between LSM100 and LSM98 and abrupt change between LSM98 and LSM95 were captured from both XPS and AES, proving the validity of these analyses.

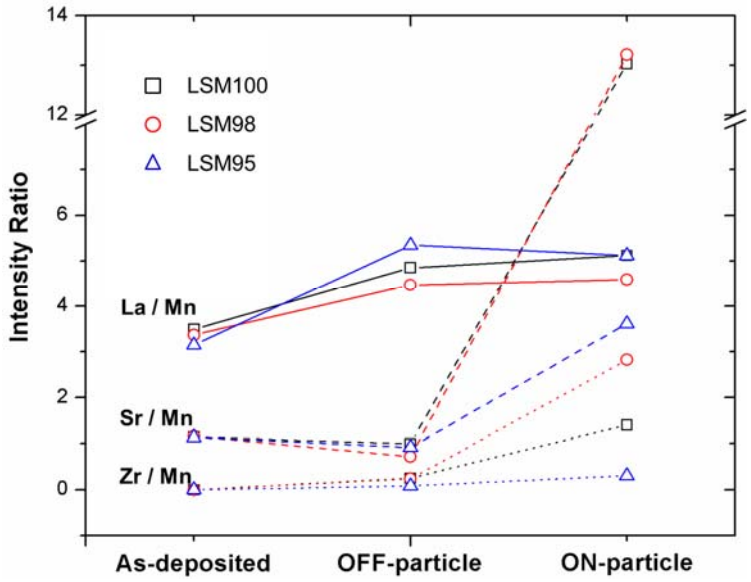

Figure 4. Cation intensity ratios of the as-deposited and annealed LSM films. Black squares, red cicles, and blue triangles represent intensity ratios from LSM100, LSM98, and LSM95, resepctively.

Nature of the surface segregation and secondary phases

Observed strong enrichment of Sr and Zr in the particles on the annealed LSM films indicates the formation of a ternary phase, likely strontium zirconate ($SrZrO_3$), on the "surface" of the cathode films. Lanthanum zirconate ($La_2Zr_2O_7$) has been widely observed at the LSM/YSZ interface upon high temperature treatments (11,12,13). It has been well-documented that the zirconate formation at the LSM/YSZ interfaces is reduced by changing the chemistry of the LSM from a stoichiometric composition to an A-site deficient LSM (1,14,15). Absence or retarded formation of lanthanum zirconates was reported from the A-site deficient LSM films, ascribing retarded zirconate formation to excess Mn content (14,15,16). Here, for the first time, we report the progression of these zirconates onto the surface of LSM thin films, which is coupled to Sr surface segregation. Annealing can boost cation dynamics (17), resulting in significant Sr surface segregation as well as Zr interdiffusion. The diffusion of these cations followed by solid-state reactions at elevated temperatures can cause the formation of these secondary chemical phases on the surface (18). We demonstrate that the A-site stoichiometry in LSM films affects the Sr segregation on the surface and phase separation, i.e., the formation of secondary chemical phases can be reduced on the surface with the A-site deficiency in the LSM films.

Significantly smaller Sr/Mn ratio on LSM95 compared to LSM100 and LSM98 substantiates the higher stability of A-site deficient LSM films against Sr segregation on the surface. This higher chemical stability can be ascribed to more space available for the cation segregation in the A-site deficient LSM films. It has been recognized that one of the major driving forces leading to the equilibrium segregation is the reduction in the elastic energy by solute segregation to the surfaces/interfaces (19). The A-site deficiency in LSM allows relatively more space available in the bulk LSM for the larger cation, Sr, and reduces the extent of Sr enrichment on the surface. This state then inhibits formation of strontium zirconate secondary phases on the surface.

Conclusions

The effects of annealing and A-site stoichiometry on the surface chemical states were investigated in dense LSM thin films with variation of A-site stoichiometry. We showed here for the first time the effects of A-site deficiency on suppressing the surface Sr segregation and the progression of secondary phase zirconate onto the surface coupled to Sr surface segregation on LSM thin films. Upon annealing, secondary phase particles were formed on the LSM surface, concurrently with Sr segregation, Zr interdiffusion, and Mn depletion. Away from those structures, however, the chemical composition remained close to that of the as-deposited LSM films with moderate changes in stoichiometry and the presence of Zr. A-site deficiency in LSM films lowered the Sr segregation and the particle density and reduced the Sr and Zr content in the particles, showing higher chemical stability against Sr segregation and the formation of the secondary chemical phases. The relatively higher stability of the A-site deficient films against Sr surface segregation is thought to be due to the excess available cation sub-lattice space in the bulk of the LSM structure that can accommodate the relatively large Sr cation more easily in the bulk, by considerations of elastic energy minimization. As a consequence of the higher chemical stability of the A-site deficient LSM thin films, we expect an improvement in the ORR kinetics and performance stability of the LSM cathodes, and the assessment of this assertion is currently in progress. Furthermore, the local electron transfer properties of these surface secondary phases are being investigated with scanning probe techniques.

Acknowledgments

The authors would like to thank the US-DOE, Office of Fossil Energy for financial support (Grant No. DE-NT0004117), and Prof. C. Ross and Prof. H. L. Tuller at MIT for the use of their PLD system.

References

1. S. B. Adler, *Chem. Rev.*, **104**, 4791 (2004).
2. Z. Cai, Y. Kuru, J. W. Han, Y. Chen, and B. Yildiz, *J. Am. Chem. Soc.*, **133**, 17696 (2011).
3. H. Dulli, P. A. Dowben, S.-H. Liou, and E. W. Plummer, *Phys. Rev. B*, **62**, R14629 (2000).
4. T. T. Fister, D. D. Fong, J. A. Eastman, P. M. Baldo, M. J. Highland, P. H. Fuoss, K. R. Balasubramaniam, J. C. Meador, and P. A. Salvador, *Appl. Phys. Lett.*, **93**, 151904 (2008).
5. NIST Database 82, U.S. Department of Commerce 2001.
6. G. J. la O', R. F. Savinell, and Y. Shao-Horn, *J. Electrochem. Soc.*, **156**, B771 (2009).
7. Z. Cai, M. Kubicek, J. Fleig, and B. Yildiz (*in review*).
8. H. Jalili, J. W. Han, Y. Kuru, Z. Cai, and B. Yildiz, *J. Phys. Chem. Lett.*, **2**, 801 (2011).
9. P. A. W. van der Heide, *Surf. Interface Anal.*, **33**, 414 (2002).
10. M. Backhaus-Ricoult, *Solid State Ion.*, **10**, 670 (2008).
11. J. A. M. Vanroosmalen and E. H. P. Cordfunke, *Solid State Ion.*, **52**, 303 (1992).
12. K. Wiik, C. R. Schmidt, S. Faaland, S. Shamsili, M. A. Einarsrud, and T. Grande, *J. Am. Ceram. Soc.*, **82**, 721 (1999).
13. K. Yang, J. H. Shen, K. Y. Yang, I. M. Huang, K. Z. Fung, and M. C. Wang, *J. Power Sources*, **159**, 63 (2006).
14. A. Mitterdorfer and L. J. Gauckler, *Solid State Ion.*, **111**, 185 (1998).
15. Y. L. Liu, A. Hagen, R. Barfod, M. Chen, H. J. Wang, F. W. Poulsen, P. V. Hendriksen, *Solid State Ion.*, **180**, 1298 (2009).
16. C.-C. T. Yang, W.-C. J. Wei, and A. Roosen, *J. Am. Ceram. Soc.*, **87**, 1110 (2004).
17. Z. Feng, C.-Y. Kim, J. W. Elam, Q. Ma, Z. Zhang, M. J. Bedzyk, *J. Am. Chem. Soc.*, **131**, 18200 (2009).
18. K. Szot and W. Speier, *Phys. Rev. B*, **60**, 5909 (1999).
19. M. F. Yan, R. M. Cannon, and H. K. Bowen, *J. Appl. Phys.*, **54**, 764 (1983).